

DOI: 10.1002/cbic.201300622

Structure-Dependent Binding of Arylimidamides to the DNA Minor Groove

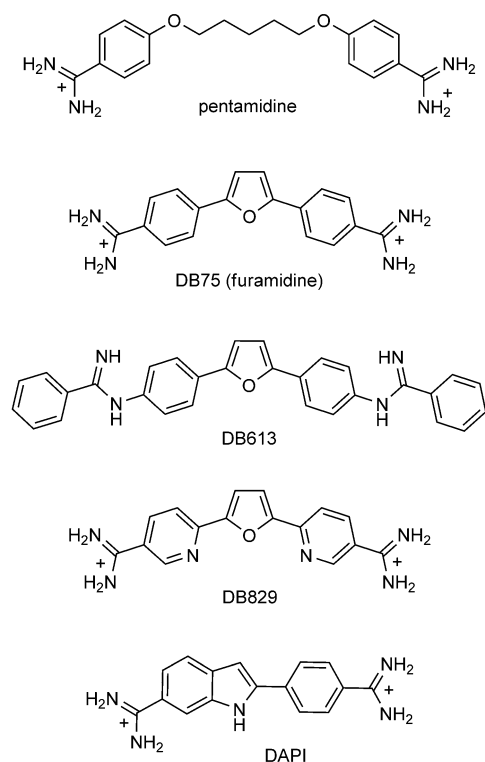
Yun Chai,^[a] Manoj Munde,^[a] Arvind Kumar,^[a] Leah Mickelson,^[a] Sen Lin,^[b] Nancy H. Campbell,^[b] Moly Banerjee,^[a] Senol Akay,^[a] Zongying Liu,^[a] Abdelbasset A. Farahat,^[a] Raja Nhili,^[c] Sabine Depauw,^[c] Marie-Hélène David-Cordonnier,^[c] Stephen Neidle,^[b] W. David Wilson,^{*,[a]} and David W. Boykin^{*,[a]}

Heterocyclic diamidines are strong DNA minor-groove binders and have excellent antiparasitic activity. To extend the biological activity of these compounds, a series of arylimidamides (AIAs) analogues, which have better uptake properties in Leishmania and *Trypanosoma cruzi* than diamidines, was prepared. The binding of the AIAs to DNA was investigated by T_m , fluorescence displacement titration, circular dichroism, DNase I footprinting, biosensor surface plasmon resonance, X-ray crys-

tallography and molecular modeling. These compounds form 1:1 complexes with AT sequences in the DNA minor groove, and the binding strength varies with substituent size, charge and polarity. These substituent-dependent structure and properties provide a SAR that can be used to estimate K values for binding to DNA in this series. The structural results and molecular modeling studies provide an explanation for the differences in binding affinities for AIAs.

Introduction

Protozoal parasitic diseases have caused significant human health problems for centuries and they continue to do so in developing countries. Chagas' disease (American trypanosomiasis) and Leishmaniasis are particularly widespread and do not currently have satisfactory treatments for the affected populations.^[1,2] Chagas' disease, caused by *Trypanosoma cruzi*, is prevalent from the southern United States to Argentina, with 90 million people estimated to be at risk and 16–18 million currently infected.^[3] Over 300 million people around the world are at risk of contracting the Leishmania parasite, and drugs used to treat that disease are also unsatisfactory: most exhibit considerable toxicity and resistance is developing.^[4,5] Aromatic diamidines, such as pentamidine (Scheme 1) are active against the *Trypanosoma brucei* parasite, which causes the sleeping sickness human African trypanosomiasis (HAT), as well as against other parasites.^[6] Highly fluorescent heterocyclic diamid-



Scheme 1. Structures of the compounds and DNA sequences used in this study. For SPR experiments, 5'-biotin labeled DNA sequences were used.

dine analogues of pentamidine have been developed, and fluorescence microscopy, as well as detailed molecular biology analysis, has demonstrated that the mitochondrial kinetoplast

[a] Dr. Y. Chai, Dr. M. Munde, Dr. A. Kumar, L. Mickelson, Dr. M. Banerjee, Dr. S. Akay, Dr. Z. Liu, Dr. A. A. Farahat, Prof. W. D. Wilson, Prof. D. W. Boykin
Department of Chemistry, Georgia State University
50 Decatur St. SE., Atlanta, GA 30303 (USA)
E-mail: wdw@gsu.edu
dboykin@gsu.edu

[b] Dr. S. Lin, Dr. N. H. Campbell, Prof. S. Neidle
The School of Pharmacy, University College London
29–39 Brunswick Square, London WC1N 1 AX (UK)

[c] Dr. R. Nhili, S. Depauw, Prof. M.-H. David-Cordonnier
INSERM U837-JPARC (Jean-Pierre Aubert Research Center)
Team Molecular and Cellular Targeting for Cancer Treatment
Université Lille Nord de France, IMPRT-IFR-114
Institut pour la Recherche sur le Cancer de Lille
Place de Verdun, 59045 Lille Cedex (France)

Supporting information for this article is available on the WWW under <http://dx.doi.org/10.1002/cbic.201300622>.

is the primary cellular target of the compounds.^[7–14] A prodrug of furamidine (DB75) has been used in clinical trials against first-stage HAT, and a related compound is active against the second stage of the disease.^[6,15–18] Clearly compounds of this type are promising for the treatment of HAT and related diseases.^[19–21]

As the heterocyclic diamidines bind to the minor groove of DNA at AT sites of four or more base pairs, and the DNA of the kinetoplast has a very large number of appropriate binding sites, targeting this unique DNA structure of the parasite offers a number of therapeutic advantages. Replication of the circular, interlocked kinetoplast DNA appears to be particularly sensitive to the diamidines, perhaps due to compound-induced conformational changes that disrupt the kinetoplast structure.^[22–24] There are no known DNA structures in humans that are equivalent to the kinetoplast, so targeting the kinetoplast offers an excellent route to selective drug action.^[11] The diamidines are taken up into *T. brucei* cells by the P2 membrane transporter, and, because the parasite lives in blood in all initial stages of infection, uptake is quite effective.^[25] These compounds are, however, taken up much less effectively by both the *T. cruzi* and Leishmania parasites that live in human macrophage cells. They still appear to target the kinetoplast of these organisms but they are much less active against them, presumably due to poor uptake.^[26]

A potentially promising route to developing new heterocyclic cations that could selectively target the kinetoplast of *T. cruzi* and Leishmania but which also have the potential for better cell uptake is to modify the amidine group while maintaining the basic structure that is the key component of the DNA interactions. A promising modification involves conversion of the amidines to arylimidamides (AIAs, previously referred to as “reverse” amidines) in which a nitrogen of the amidine is linked to the heteroaromatic core (Table 1) rather than the carbon in classical amidines (Scheme 1). The AIAs have lower pK_a values and typically have much better biological activity against both *T. cruzi* and Leishmania than the amidines.^[27–31] The AIAs offer a new approach for the development of drugs against these diseases, but we understand much less about their DNA interactions than those of amidine derivatives. As a key step in understanding their biological targets as well as developing these compounds to effectively treat parasites, we have evaluated the interactions of an array of modified AIAs with AT DNA binding sites that are typical of those found in kinetoplast DNA. This is the first detailed study of DNA complexes of AIAs, and the results show a surprisingly large variation in DNA interactions with relatively small changes in the structure of the compounds.

Results and Discussion

Thermal melting: Ranking the compounds

Thermal melting enables rapid qualitative evaluation of the relative binding affinities of compounds for DNA.^[32] As part of a screen to find new compounds that target kinetoplast AT sequences, ΔT_m values for AIAs with poly(dA)·poly(dT) were

Table 1. Comparison of T_m and fluorescence for AIAs.			
Compound	R	ΔT_m [a] [°C]	F_{70} [b] [μ M]
DB667	H	19.6	1.7
DB709	OCH ₃	13.1	1.2
DB745	OCH ₂ CH ₃	8.1	2.0
DB766	OCH(CH ₃) ₂	6.0	5.5
DB1890	OCH ₂ CH(CH ₃) ₂	2.0	> 10
DB1950	OCH ₂ CH ₂ CH(CH ₃) ₂	1.0	> 10
DB1852		0.2	> 10
DB1880		27.1	0.55
DB1876		25.0	0.6
DB766		6.0	5.5
DB1831		7.0	1.2
DB1855		1.1	9.0
DB1937		0.5	> 10

[a] Poly(dA)·poly(dT), values are an average of three independent trials with a reproducibility of ± 0.5 °C. [b] The compound concentration required to reduce the fluorescence of DAPI in complex with A₅ to 70% of the initial value. The values are reproducible within 10%.

determined (Table 1). The ΔT_m values of the DNA complexes show quite large, structure-dependent variations. Triple helix formation (TnAnTn) was excluded because it leads to biphasic melting curves for the duplex and triplex species. As biphasic curves were not seen with the AIAs (Figure S1 in the Supporting Information), and as duplex-specific minor groove binders are usually very poor triplex inducers, we are able to rule out any triplex formation.^[33]

O-Alkyl substitution: Scaffold A: The R group in scaffold A of Table 1 has O-alkyl substituents of increasing size or piperidine groups with two extra charges. The ΔT_m values are quite sensitive to compound structure. With the unsubstituted DB667 (R=H), for example, $\Delta T_m = 19.6$ °C, but as the alkyl group increases in size, there is a large decrease in the ΔT_m . With an OMe R group, DB709, ΔT_m is down to 13.1 °C, and the compound with an OCH₂CH(CH₃)₂ group, DB1890, has a ΔT_m of only 2.0 °C. DB1880 with a charged O-piperidine group and DB1876 with a charged O-isopropylpiperidine group, on the

other hand, have very high ΔT_m values despite the substantial size of the substituent.

Variations in the terminal six-membered rings: Scaffold B: Compounds in scaffold B have extra nitrogen atoms added to the terminal pyridine of DB766, and their ΔT_m values are sensitive to the N position (Table 1). The ΔT_m values are relatively low for all compounds in the scaffold B group.

Fluorescence displacement titrations: Comparing the relative affinities

Unlike classical amidines, AIAs do not fluoresce by themselves, therefore, fluorescence-displacement titrations were used as an additional screen to rank them according to their binding affinity at 25 °C rather than the high temperatures in T_m experiments. The compounds were tested with hairpin DNAs containing an A_5 binding sequence, which is an analogue of the poly(dA)-poly(dT) used in T_m experiments, and an ATATA sequence to evaluate the AT-sequence-dependent interactions with DNA. DNAs with two fluorophores, DAPI and DB829, (Scheme 1), which have very different properties, were used to test the binding affinities. DAPI alone has low fluorescence, but when bound to DNA it fluoresces strongly, whereas DB829 has the reverse fluorescence behavior. Figure 1A, B shows typical fluorescence-displacement titrations with DB1876 for DAPI- A_5 and DB829- A_5 complexes. Titration of the DAPI- A_5 complex with DB1876 displaces DAPI and results in a decrease in the intensity, as expected. The opposite change in fluorescence is observed upon titration of the DB829 complex. Figure 1C, D compares ratio plots for titration of A_5 -DAPI and A_5 -DB829 with several compounds from Table 1. The titration displacement curve for DB1876 is sharp and the compound displaces DAPI and DB829 at low compound concentration. F_{70} , the compound concentration required to reduce the fluorescence to 70% of the initial value, for DB1876 is 0.6 (all concentration values in μM) with DAPI- A_5 , whereas the values for the other compounds in the plot are higher: $F_{70}=1.2$ (DB709), $F_{70}=5.5$ (DB766), and $F_{70}>10$ (DB1852). The displacement results with DB829 are in general agreement with the DAPI and T_m results.

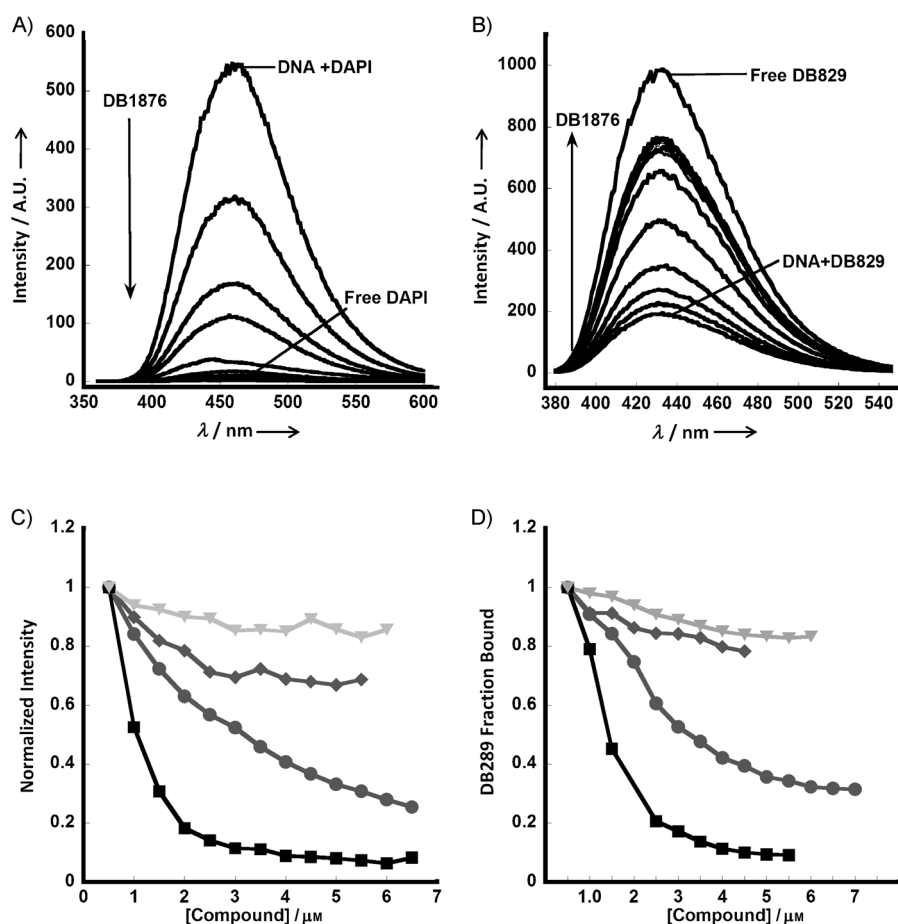


Figure 1. Fluorescence displacement titrations. Titration of DB1876 into A) DAPI- A_5 and B) DB829- A_5 hairpin DNA complexes. DAPI fluoresces when bound, so as it is displaced, fluorescence intensity decreases. DB829 fluoresces more strongly in solution, so as it is displaced, the fluorescence intensity increases. Normalized fluorescence displacement titration. Representative normalized plots of intensity vs. compound concentration for fluorescence displacement titration of DB1876 (■), DB1852 (▼), DB766 (◆) and DB709 (●) titrated into C) DAPI- A_5 and D) DB829- A_5 complexes. DB1876 has the highest binding affinity; DB709 has a moderately high binding affinity; DB766 and DB1852 have low binding affinity.

The agreement between the ΔT_m and F_{70} results is illustrated with the plots in Figure 2 for the compounds in Table 1. The fluorescence displacement titration results are in excellent agreement with the inverse of the ΔT_m values. Both sets of re-

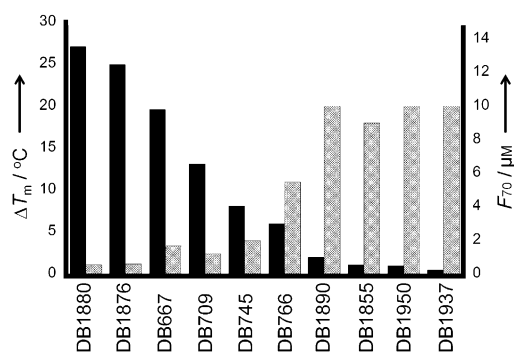


Figure 2. Comparative histogram plots of ΔT_m (■) and fluorescence (▨) for some compounds that vary significantly in DNA affinity.

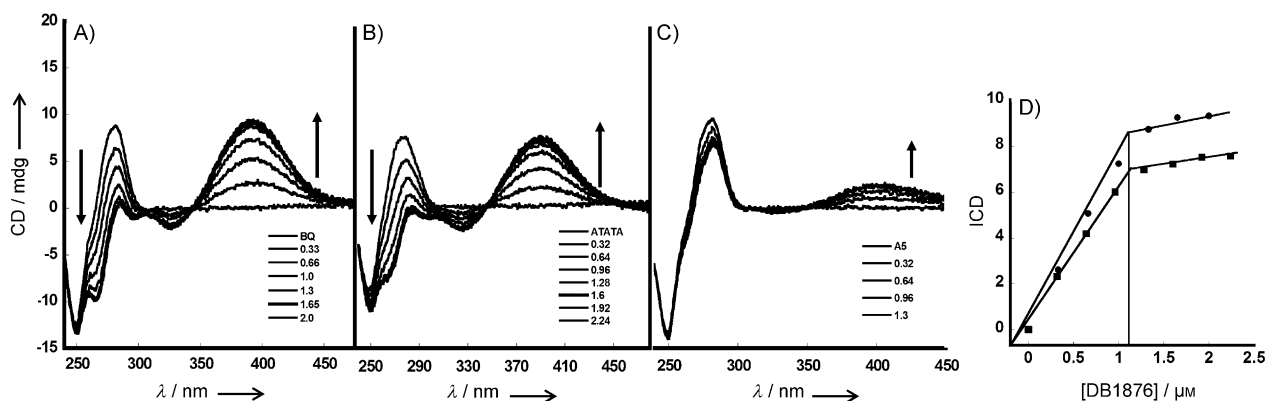


Figure 3. Circular dichroism spectra of A) DB1876–A₅, B) DB1876–ATATA, and C) DB1852–A₅ titrations for added ratios (compound to DNA hairpin) ranging from bottom to top from 0.32 to 3.0. D) A plot of induced CD (ICD) versus DB1876/DNA ratio; ●: A₅, ■: ATATA.

sults show that the AIAs bind to AT DNA sequences in a structure-dependent manner, and some compounds bind quite strongly.

CD: Determining the binding mode and stoichiometry

CD spectroscopy with A₅ and ATATA hairpin DNA sequences was used to obtain information on the binding mode of AIA compounds that were selected based on T_m and F_{70} results (Figure 3). Positive induced signals in CD spectroscopy are generally obtained for compounds that bind in the DNA minor groove, and this pattern provides a method for evaluating binding modes. DB1876 gives strong induced CD with saturation at a compound to DNA ratio of about 1:1. A plot (Figure 3D) of induced CD (ICD) versus compound/DNA ratio indicates a break at approximately 1:1 for A₅ and ATATA and suggests that DB1876 binds as a monomer in the minor groove of these AT sequences. With A₅ it is also possible to fit the data differently, with a break at a 1.4:1 ratio. Because these simple oligomers should bind the compound at either a 1:1 or 1:2 ratio, we think the fit at near the 1:1 ratio is more reasonable. DB1852, a close analogue of DB1876 with a neutral *O*-pentacyclic ring, shows poor CD, thus indicating that it binds weakly, in agreement with T_m and F_{70} results. The CD results thus confirm a minor groove binding mode for the compounds of Figure 1A, B and generally support the T_m and F_{70} conclusions.

SPR biosensor: Quantitative and stoichiometric analysis of complexes

In order to evaluate the interactions of representative AIA analogues with DNA more quantitatively, biosensor-SPR experiments were conducted with DNA hairpin duplexes containing A₅ and ATATA sequences. The flow cells for A₅ and ATATA had essentially the same amount of DNA immobilized so that their sensorgram saturation levels could be com-

pared directly for stoichiometry differences. The sensorgrams of DB667 (Figure 4A) show fast kinetics of association and dissociation and they can be fitted to a steady-state analysis.^[34–36] The steady-state values (in response units, RU) were plotted against C_{free} (free compound concentration) and fitted to a single site model (Figure 4D) that is predicted by the RU value at saturation of the DNA binding site.^[37] The values of the equilibrium binding constant, K , are collected in Table 2. DB667 binds strongly to A₅ ($9.0 \times 10^6 \text{ M}^{-1}$) and somewhat more weakly to ATATA ($2.8 \times 10^6 \text{ M}^{-1}$). Interestingly, DB709, with –OMe groups in place of the –H in DB667, has significantly reduced affinity (Figure 4C, F). DB766, which was difficult to study due to poor binding and water solubility, shows very low SPR signals (data not shown) that confirm its weaker binding affinity.

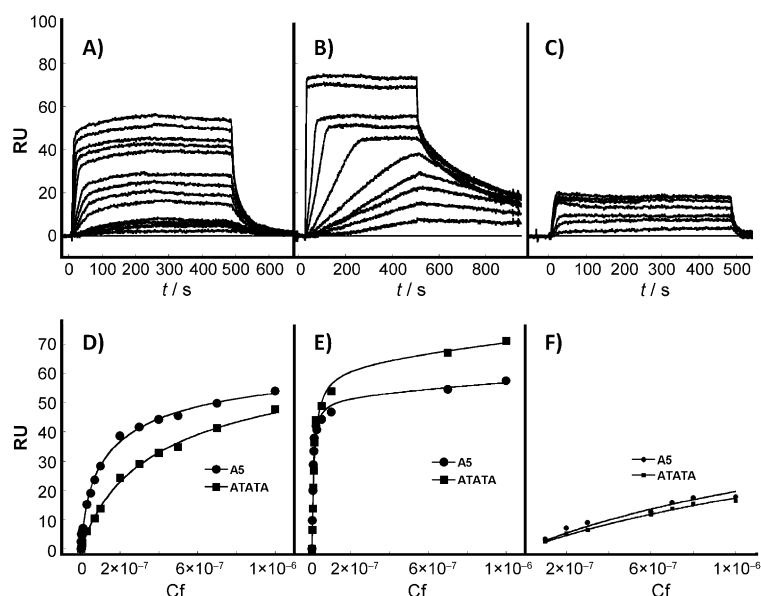


Figure 4. Surface plasmon resonance. Representative SPR sensorgrams for: A) DB667, B) DB1876, and C) DB709 binding to immobilized A₅ and ATATA hairpin DNAs. The compound concentrations were 0.01 to 1.0 μM from bottom to top. SPR binding affinity plots. RU values from the steady-state region of SPR sensorgrams are plotted against the unbound compound concentration, C_{free} (flow solution) for D) DB667, E) DB1876, and F) DB709 with A₅ (●) and ATATA (■) DNA.

Table 2. Selected SPR binding affinities.^[a]

Compound	K [10^6 M^{-1}]		Compound	K [10^6 M^{-1}]	
	A_5	ATATA		A_5	ATATA
DB75 ^[23]	18	24	DB709	0.5	0.4
DB613	15	3.6	DB1876	85	57
DB667	9.0	2.8			

[a] The listed binding affinities are an average of two independent experiments carried out with two different sensor chips, and the values are reproducible within 10%.

Sensorgrams for DB1876, with the *O*-isopropylpiperidine ring, show that the compound has much slower binding kinetics with DNA than the other AIAs (Figure 4B). At low compound concentrations, the slow kinetics prevent a steady state from being reached within the experimental time range, which is limited by injection volume. Even for these low-concentration samples, it is possible to fit the curves to a 1:1 kinetic binding model^[33–36] to determine predicted steady-state RU values for DB1876. At higher concentrations of DB1876, a steady state was reached, and these values can be used directly in RU versus C_{free} plots along with predicted values (Figure 4E). DB1876 has very strong binding affinity for A_5 and somewhat weaker binding to ATATA (Table 2). These results are in excellent agreement with the more qualitative T_m and fluorescence results.

DNase I footprinting: Sequence specificity

To compare the binding of compounds with high-molecular-weight DNA to the results obtained with the hairpin DNAs, DNase I footprinting studies were conducted. DNase I cuts DNA at all sites but with variations in rates that depend on the local minor-groove geometry. Small molecules that bind in the minor groove block access of the enzyme and result in reduced cleavage.^[38,39]

Footprinting results for selected AIAs from Table 1 are shown in Figure 5 with an experimental gel. DB75, a well-characterized diamidine, was used as a control in these studies and displays good footprints at both the alternating and nonalternating AT sequences. Gel results for DB766 show no detectable footprint up to $> 1 \mu\text{M}$. The more highly charged DB1876 has strong footprints at $0.5 \mu\text{M}$ and above, whereas DB1880 (*O*-piperidine) has strong footprints at $0.25 \mu\text{M}$ and above. These results are in agreement with the T_m and SPR results and suggest that the hairpin DNAs' affinities reflect those of the higher-molecular-weight DNAs.

X-ray crystallography: The structure of the DB1880–DNA complex

In order to evaluate the structural basis of AIA–DNA minor-groove complexes as well as strong binding of the tetracationic derivatives, crystals of the DB1880–DNA complex were grown, and its structure was solved by X-ray crystallography. The $d(\text{CGCGAATTCGCG})_2$ sequence forms a self-complementary

B-form DNA duplex helix, as observed in a large number of previous studies.^[40–43] The helically twisted DB1880 molecule is bound as a monomer in the minor groove and covers almost all of the 6-bp sequence (A5/T20) (A6/T19) (T7/A18) (T8/A17) (C9/G16) (G10/C15) in this narrow central region of the helix (Figure 6A, B). The two phenyl rings and the furan ring are oriented parallel to the walls of the minor groove and are deeply embedded, whereas the two terminal pyridine rings are twisted to the mean plane of these three central rings and are close to the mouth of the minor groove.

There are a number of direct hydrogen-bond and water bridging contacts between the ligand and the DNA, as shown in Figure 6B. One inward-facing amidine nitrogen atom is oriented out of the plane of the central diphenylfuran moiety by 43° and hydrogen bonds to the O2 atoms of T20 and T19 (2.7 and 3.3 Å, respectively). This nitrogen atom is also involved in hydrogen bonding to the O4' atom T20 (3.0 Å) (Figure 6C). At the other end of the DB1880 molecule (Figure 6D), the amidinium group is twisted by 72° relative to this plane, and one amidinium nitrogen atom hydrogen bonds to the O2 (2.7 Å) and O4' atoms (3.0 Å) of C9. The other amidinium nitrogen atom is involved in hydrogen bonding to the O4' atom of A18 (3.2 Å) on the complementary strand.

Neither piperidinyll group directly hydrogen bonds to the DNA. One interacts through its nitrogen atom, via a bridging water molecule, to a phosphate group, as does the adjacent pyridine ring, to the next phosphate group on the same strand. The latter water molecule also hydrogen bonds to the adjacent amidinium nitrogen atom as well as to a short chain of water molecules that links to a third phosphate group (Figure 6E). Both piperidine groups extend outwards from the groove so that their cationic ring nitrogen atoms are relatively close to the anionic phosphate groups. Although few water molecules have been located in the vicinity of these nitrogen atoms, we cannot discount the possibility that the water bridging referred to above occurs more extensively; indeed, there is a strong likelihood that further water molecules are present in these regions.

A well-pronounced network of water molecules is apparent, surrounding the outer edge of the bound ligand. This horse-shoe-like arrangement extends along the phosphate groups of both strands and terminates at one end of the ligand in a network of two connected rings of water molecules, closely similar to previous observations of water networks in DNA minor-groove–ligand complexes.^[44]

Free compound modeling and docking with DNA

In order to better understand the effects of substituents on AIA–DNA interactions molecular docking studies were performed.

O-Alkyl substitution: *Scaffold A*: With the unsubstituted DB667 ($R=\text{H}$, Table 1), DFT calculations for optimizing geometry at the 631G* approximation level shows that the phenyl–furan–phenyl system adopts a coplanar conformation (Figure 7A). As the alkyl group increases in size with the addition of *O*-alkyl substituents, steric hindrance overcomes the long-

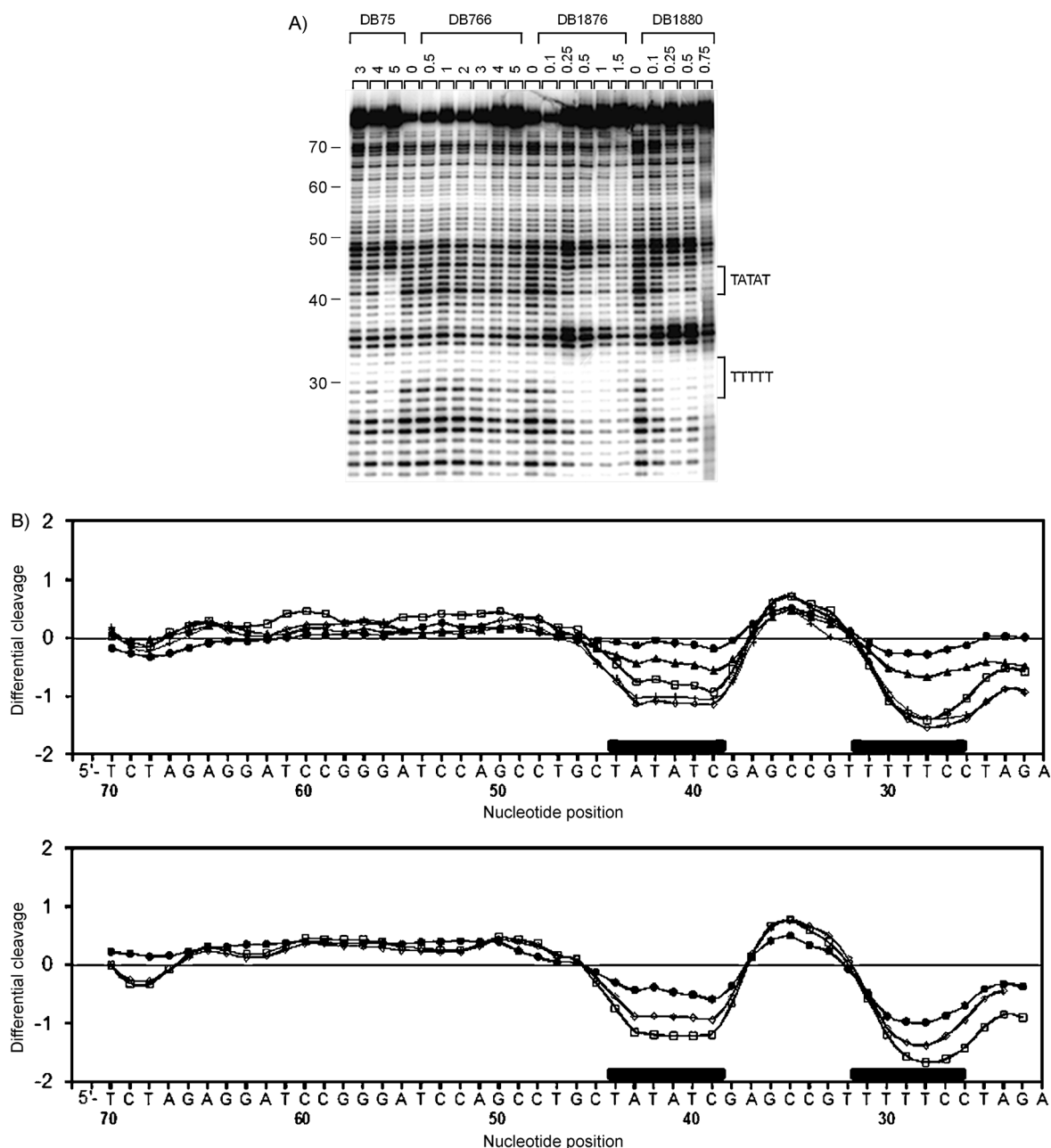


Figure 5. DNase I footprinting titration experiments. The 81 bp DNA fragment containing A₅ and ATATA sites was incubated with increasing concentrations [μM] of DB75, DB766, DB1876, and DB1880 prior to being subjected to mild digestion with DNase I. A) The digested products were separated on a 8% polyacrylamide gel containing 8 M urea. Sequences at the footprinting sites are indicated to the right of the gel. B) Corresponding densitometric analysis reveals the localization of the footprints (black boxes) along the DNA sequence. Top: 0.1 (●), 0.25 (□), 0.5 (◇), 0.75 (▲), 1 μM (+) DB1876; bottom: 0.1 (●), 0.25 (□), 0.5 μM (◇) DB1880.

range conjugation and causes some twist between the phenyls and furan. DB1890, which has R=OCH₂CH(CH₃)₂, for example, has dihedral angles between the phenyl and furan ring of approximately 14°.

DB613 (Scheme 1) has the same central phenyl–furan–phenyl rings but with terminal substituted phenyl groups instead of the pyridine in DB667. The dihedral angles between the AIA and the terminal phenyl or pyridinyl planes are 37° and 4° in DB613 and DB667, respectively. The modeling results suggest that the close planarity of the terminal pyridinyl

groups and amidine group in DB667 could be due to their ability to form amidine group...pyridine hydrogen bonds. Meanwhile in DB613, rotation of terminal phenyl rings into the AIA plane is more hindered by van der Waals repulsion between the hydrogen atoms, and a H-bond is not possible.

Molecular electrostatic potential (MEP) maps illustrate the charge distributions of molecules, help to understand the relative polarity of a molecule, and are useful for evaluating structure–activity relationships. The maps clearly show a significantly different distribution of MEPs for the compounds (Figure 7A).

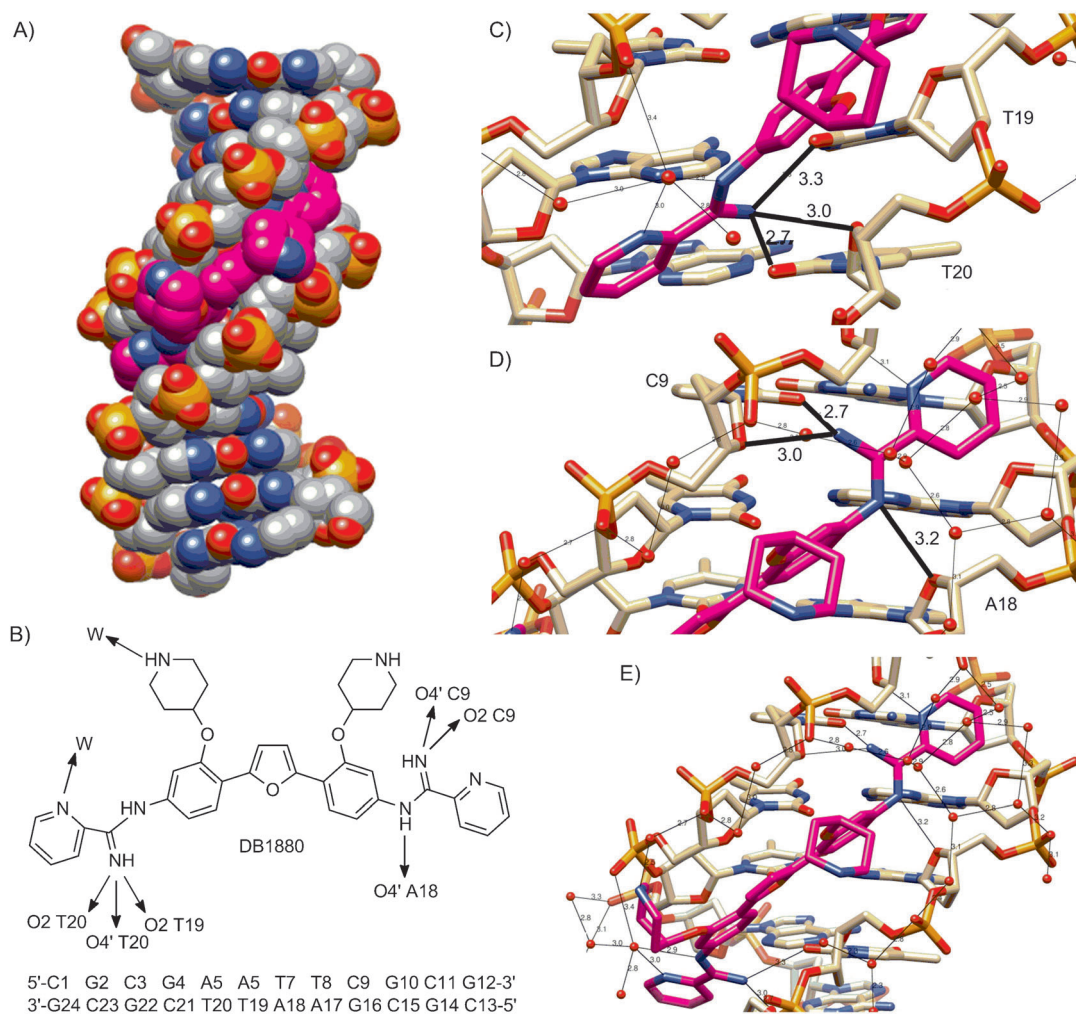


Figure 6. A) Crystallographic structure of the DB1880–DNA complex. The DNA sequence is shown in gray, DB1880 molecule in magenta, nitrogen atoms in blue, and oxygen atoms in red. B) The full sequence with bases numbered and binding schematic. Detailed views of the hydrogen-bonding interactions between DB1880 and DNA. The distances [Å] were measured between heavy atoms. C) The three hydrogen bonds between one amidinium nitrogen atom and the oxygen atoms of T19 and T20. D) The hydrogen bonds between two amidinium nitrogen atoms and the oxygen atoms of C9 and A18. E) The network of hydrogen bonds bridging water molecules between DB1880 and DNA phosphate oxygen atoms.

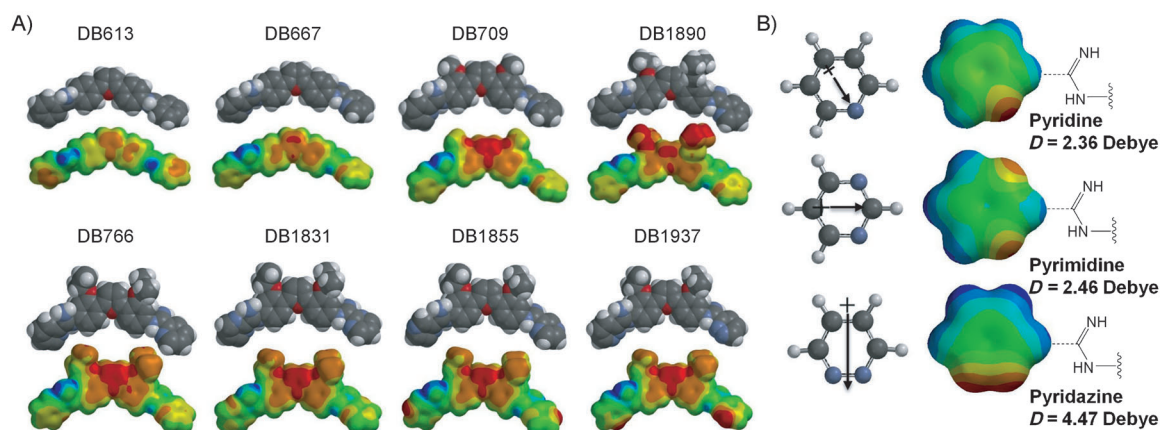


Figure 7. A) Electrostatic potential maps. Equilibrium geometry of the AIAs calculated by the DFT B3LYP approximation at the 631G* level. Space-filling models are shown at the top, with electrostatic potential molecular surfaces at the bottom; blue=positive and red=negative potential, the color was set at the same scale. B) Comparison of dipole moments. Ab initio-calculated electrostatic potential maps for the pyridine, pyrimidine and pyridazine units of DB766, DB1831 and DB1937, respectively. The dipole moments of these units are shown on the left; the magnitudes of the dipoles are on the right.

As expected, the negative potential is stronger on oxygen atoms, whereas the positive potential is stronger on the amidine –NH groups. The inner faces of the molecules, towards the floor of the minor groove, have a positive character. The outer face, towards the solvent, is relatively more negatively charged. This favors the formation of hydrogen bonds and electrostatic interactions between bases at the floor of the DNA minor groove and AT sequences. With large O-alkyl groups on the inner phenyl rings, such as with DB1890, the negative potential is predicted to be partially shifted from the furan ring to the alkyl substituents.

Molecular-docking studies can provide ideas for variations in binding affinity across a set of derivatives such as the AIAs and are particularly powerful if guided by X-ray structural results, such as those with DB1880. The results obtained from molecular docking indicate that DB667 binds as a monomer in the center of the minor groove of the d(CGCGAATTCGCG)₂ duplex (Figure 8A) and covers almost six base pairs. This orientation

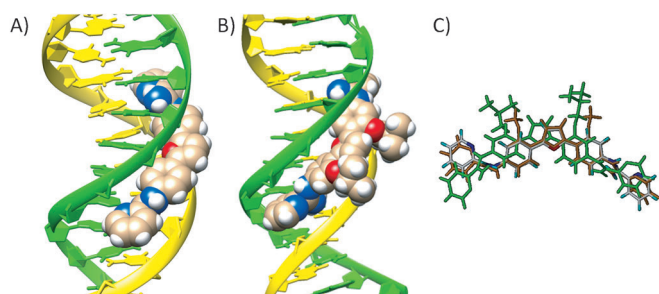


Figure 8. Molecular docking. Models of complexes of A) DB667 and B) DB1890 with the DNA duplex dodecamer sequence d(CGCGAA TTCGCG)₂ given the X-ray crystal structure 3OIE as a guide. C) Overlay of the structures of DB667, DB709 and DB1890 docked into the same DNA sequence. DB667 is displayed by atom type color, DB1890 is green, and DB709 is brown.

fits snugly in the DNA minor groove, and the inward-facing amidinium nitrogen atoms are involved in hydrogen bonding to the cytosine and thymine O2 groups. Docking of DB709 into the same DNA sequence gave similar results. As the alkyl substituent increases in size, the substituted compound no longer fits properly into the minor groove for optimum binding. Steric hindrance and unfavorable electrostatic contacts of the substituents with the minor groove limit binding. An example docking result for DB1890 is shown in Figure 8B. The phenylfuran core is pushed away from the floor of the groove, and all interactions with the DNA are weakened. An overlay of DB667 and DB1890, which were extracted from an overlay of their DNA complexes after deletion of DNA, is shown in Figure 8C. The suboptimal binding position of DB1890—pushed out and down the groove—can be seen in this comparison.

Variations in the terminal six-membered rings: Scaffold B: Addition of a nitrogen atom to the terminal pyridine of DB766 gives scaffold B compounds, which show electrostatic potential maps that are sensitive to the N position (Figure 7A). For DB1831 (R=pyrimidine, Table 1), the dihedral angle between the amidine groups and the terminal pyrimidinyl plane is 0°, compared to 4–6° in the other three compounds. This differ-

ence is perhaps due to the ability to form two amidine–pyrimidinyl hydrogen bonds and to the elimination of repulsive CH van der Waals interactions with the amidine group in DB1831. The electrostatic potential molecular surfaces of the central aromatic system on DB766, DB1831, DB1855 (R=pyrazine), and DB1937 (R=pyridazine) are similar; however, the MEP map clearly shows a significantly different distribution on the terminal rings. In DB1855 and DB1937, the significantly negative potential centralizes on the terminal pyrazinyl or pyridazinyl nitrogen atoms, whereas the electrostatic potential is more evenly spread across the pyridinyl and pyrimidinyl systems in DB766 and DB1831. This quite polar region in DB1855 and DB1937 attracts the bonding electrons more strongly and provides a greater attractive force for the aqueous proton. In an aqueous environment, all four compounds have bound water molecules around them, and some of these water molecules need to be released in order to bind to DNA. As the pyridazinyl group in DB1937 would attract bound water molecules more tightly than DB766 and DB1831, more energy is required to release the same number of water molecules and this could be a factor in explaining the different binding affinities. A contribution from a pK effect is also possible and could reflect a partial lack of protonation of the amidine groups under the test conditions; this would greatly affect DNA binding affinity.

In order to better understand the energy contributions, it is important to compare the ab initio calculated MEP for the terminal heterocyclic units (Figure 7B). The pyridazine ring in DB1937 possesses a high dipole moment (4.47 D), which is attributed to the fact that the two nitrogen atoms are located on the same side of the ring. Therefore, there is a greater pull of electrons to that side that results in a high dipole moment. The dipole moment of pyrazine is 0 since it is symmetrical about the line passing two nitrogen atoms. The higher magnitude of dipole moment for pyridazine, compared to pyridine (2.36 D) and pyrimidine (2.46 D), suggests a possible contribution toward the lower observed binding affinity of DB1937. Intermolecular attractions in pyridazine are stronger than in pyridine and pyrimidine; this is attributed to electrostatic forces arising from the high permanent dipole.

Conclusions

It is useful to put the results on DNA binding of the AIA compounds reported here in context relative to other similar minor-groove-binding dications. The binding of the diphenylfuran diamidine, DB75, which has the same central aromatic system as the AIAs in Table 1, to both the A₅ and ATATA sequences has been extensively characterized.^[23] This compound has an equilibrium constant of approximately $2 \times 10^7 \text{ M}^{-1}$ with both DNAs. DB613, which has the same central diphenylfuran but with a phenyl group instead of the pyridine in DB667, has been evaluated with the same DNA sequences and has a similar *K* to DB75 for A₅ but one that is nearly seven times lower with ATATA (Table 2). DB667 has slightly lower *K* values than DB613 with both DNAs. Interestingly, most amidine and AIA derivatives bind more poorly to the ATATA sequence than to A₅, and it is actually DB75 that is unusual for its similar binding to the

two DNAs. The weaker binding to ATATA in general can be explained by the wider minor groove with that sequence relative to A₅.^[7,23] Molecular modeling with an AATT sequence that has been crystalized with both amidines and AIAs shows that DB613 and DB667 can be inserted into the minor groove in much the same manner as DB75 in the AATT site (Figure 8).

Replacement of the central phenyl hydrogen atom in DB667 by larger groups decreases the ΔT_m values and increases the amount of compound required to displace DAPI from the minor groove (Table 1). Adding $-\text{OCH}_3$, in an otherwise equivalent compound (DB709), gives a reduction in ΔT_m of 6–7 °C, and substitution with *O*-isopropyl (DB766) causes another 6–7 °C decrease. Larger OR substituents have ΔT_m values that approach 0 °C (Table 1). Molecular modeling and docking of these compounds in the minor groove provides a clear rationale for the decrease in T_m with larger substituents (Figure 8). The large substituents are significantly out of the conjugated phenyl–furan ring plane and, as shown in Figure 8, they prevent the attached compounds from penetrating as deeply into the groove as compounds that have smaller substituents. This weakens H-bond interactions with the base edges at the floor of the groove and van der Waals contacts to the walls of the groove in the complex.

Several compounds were prepared with an additional N in different positions of the terminal pyridyl of DB766. The pyrimidine, DB1831, has essentially the same ΔT_m as DB766 but the other two compounds with two N atoms have substantially reduced ΔT_m values. Modeling of the compounds again provides suggestions as to why the selective decrease in T_m occurs. As can be seen in Figure 7B, the electron density of the pyrimidine in DB1831 is more evenly spread than in pyridazine, and pyrimidine has a lower dipole moment. If the nitrogens of the pyridazine in DB1937 face into the AT minor groove, this quite polar region will be dehydrated and will have no possible H-bond donors. If the group faces outwards, the regions of negative potential will be near the anionic backbone of the DNA, another unfavorable binding orientation.

DB1876 and DB1880 are unique in the AIA compound set. The piperidine substituent is relatively large, at least comparable to the cyclopentyl on DB1852, but DB1880 and DB1876 have the highest binding constants of the compounds in Table 1. The two additional charges on DB1880 and DB1876 certainly help binding, but their effect is mitigated to a certain extent by the 0.1 M added NaCl in the experiments. In the crystal structure of the DB1880–DNA complex, both piperidine groups extend outwards from the groove, so that the charged piperidine $-\text{NH}$ atoms are relatively close to DNA phosphate groups, and this interaction is certainly favorable for binding. However, neither piperidyl group directly hydrogen bonds to the DNA. The very hydrophobic *O*-cyclopentyl in DB1852 clearly does not favorably interact with the minor groove in a similar way.

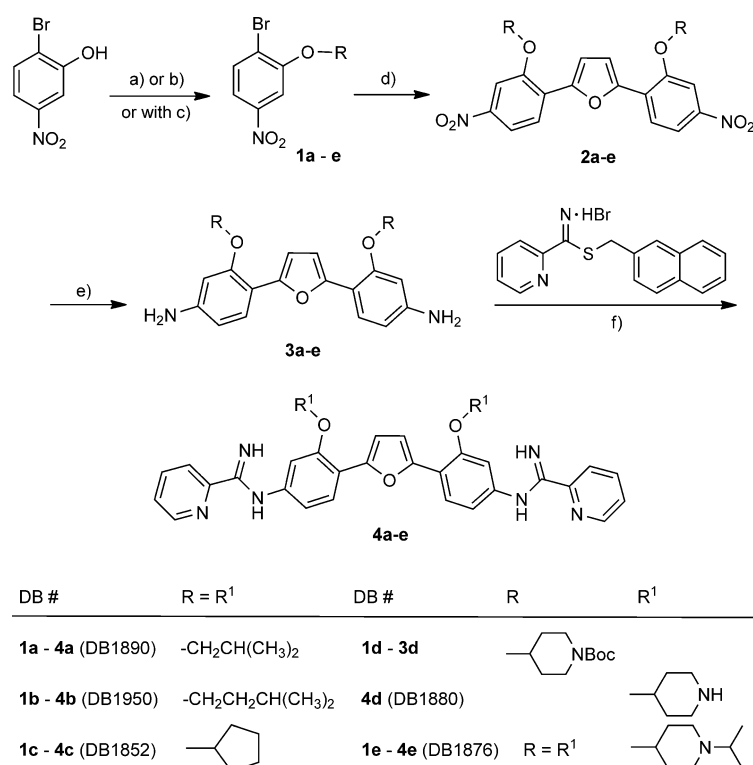
In summary, the AIAs form 1:1 complexes in AT sequences of four to six base pairs and bind with affinities that strongly depend on substituent size, charge and polarity.

Experimental Section

Compounds, DNAs, and buffers

Syntheses of the compounds of Table 1: Syntheses of DB667, DB709, DB745 and DB766 have been published,^[29,45] syntheses of compounds DB1831, DB1855 and DB1937 will be published elsewhere; and all other AIAs are described below. All synthetic compounds were characterized by ¹H and ¹³C NMR and elemental analysis (C, H, N within $\pm 0.4\%$). Poly(dA)₅·poly(dT) obtained from Pharmacia Co. was used for T_m experiments. In circular dichroism (CD) and fluorescence experiments, the hairpin DNA oligomers A₅ (5'-GCCAA AAAGC TCTCG CTTT TGGC-3') and ATATA (5'-GCCAT ATAGC TCTCG CTATA TGGC-3') with the hairpin loop sequences underlined were used (DNA sequences shown in Scheme 1). In SPR experiments, the same hairpin DNA oligomers 5'-labeled with biotin were used. The cacodylic acid buffer (CAC) used in T_m , CD, and fluorescence experiments contained cacodylic acid (0.01 M), NaCl (0.1 M), and EDTA (0.001 M) and was adjusted to pH 6.25. The SPR experiments were conducted in filtered, degassed CAC buffer with 0.005% P20 surfactant. All DNA oligomers were purchased from Integrated DNA Technologies, Inc. (Coraville, IA), purified by reversed-phased HPLC, and characterized by mass spectrometry.

Preparation of AIAs: The synthetic route to the new compounds in this paper is shown in Scheme 2. Experimental details and characterization data for all the compounds and intermediates can be



Scheme 2. Synthesis of the AIAs. a) RI, tBuOK, THF, DMF; b) i: 4-hydroxypiperidine, (Boc)₂O, Et₃N, CH₂Cl₂; ii: DEAD/PPh₃, THF; c) i: 20 mol% CF₃COOH, CH₂Cl₂; ii: 2-iodopropane, K₂CO₃, DMF; d) 2,5-bis(trimethylstannyl)furan, Pd(PPh₃)₄, dioxane; e) 10% Pd/C, H₂, 345 kPa, EtOAc/EtOH (9:1); f) i: MeCN, EtOH, RT, 24 h; ii: ethanolic HCl.

found in the Supporting Information. Starting from 2-bromo-5-nitrophenol, 1-bromo-2-alkoxy-4-nitrobenzene (**1a–d**) was prepared by treatment with either alkyl iodide or *tert*-butyl 4-hydroxypiperidine-1-carboxylate. In the case of compound **1e**, the bis-Boc-protecting groups of **1d** were first removed by using trifluoroacetic acid in CH_2Cl_2 and then treated with 2-iodopropane. Stille coupling of **1a–e** and 2,5-bis(trimethylstannyl)furan in the presence of $\text{Pd}(\text{PPh}_3)_4$ in dioxane gave the corresponding 2,5-bis(2-alkoxy-4-nitrophenyl)furans (**2a–e**). Furans **2a–e** were then reduced by catalytic hydrogenation to give the desired diamino compounds **3a–e**. The target AIA salts DB1890, DB1950, DB1852, DB1880 and DB1876 (**4a–e**) were prepared in a two-step process. First, the free base was obtained by treating **3a–e** with a hydrobromide salt of naphthalen-2-ylmethyl pyridine-2-carbimidodithioate in ethanol/acetonitrile. The free bases were subsequently treated with anhydrous ethanolic HCl to give the AIA salts in good overall yield. In the case of **4d** (DB1880), Boc-deprotection was accomplished in the process of the AIA hydrochloride salt formation.

Thermal melting (T_m): T_m experiments were conducted on a Cary 300 Bio UV/Vis spectrophotometer (Varian) with the software supplied with the instrument. A thermistor fixed into a reference cuvette was used to monitor the temperature with a computer-controlled heating rate of $0.5\text{ }^\circ\text{C min}^{-1}$. The oligomers were added to CAC buffer (1 mL) in 1 cm path-length, reduced volume quartz cells; DNA without compound was used as a control. The concentrations of the DNA solutions were determined by measuring the absorbance at 260 nm. Experiments were generally conducted at a concentration of $2 \times 10^{-5}\text{ M}$ base pair for poly(dA)-poly(dT). For experiments with complexes, a ratio of 0.3 compounds per base pair was generally used.

Fluorescence: All experiments were conducted on a Cary Eclipse Fluorimeter (Varian). Before conducting the fluorescence displacement titration for DNA–AIA complexes, it was important to find the concentration of the fluorophore (DAPI/DB829, in Scheme 1) in each experiment so that addition of the test compound would displace it. DNA (50 μM stock solution) was titrated into the fluorophore-containing cell at 0.05 μM increments, and scans were recorded. A steady change in fluorescent intensity was observed until saturation at 0.8 μM A_5 with 0.5 μM DAPI, or 2.2 μM A_5 with 0.5 μM DB829. These fluorophore concentrations were then used in each fluorescence displacement experiment.

In the fluorescence displacement assay, the DNA–fluorophore complexes were titrated with each test compound at increments of 0.5 μL (0.5 μM compound stock solutions). λ_{ex} was set to 342 nm for DAPI and to 363 nm for DB829. For DAPI, a 2.5 nm (excitation and emission) slit width was chosen, and for DB829 it was 5.0 nm. The fluorescence intensity at maximum peak was recorded for each scan. In order to compare the two assays, they were plotted as ratio values [Eqs. (1a) and (1b)]:

$$R_{\text{DAPI}} = F/F_{\text{max}} \quad (1a)$$

$$R_{\text{DB829}} = F_{\text{min}}/F \quad (1b)$$

here F is the observed fluorescence at each point, F_{min} and F_{max} are the minimum and maximum intensities in each titration, and each titration starts at a ratio of 1.0.

Circular dichroism spectroscopy: CD spectra were obtained on a computer-controlled Jasco J-710 spectrometer in 1 cm quartz cells. Typically, a buffered solution of DNA hairpin at a strand concentration of 3 μM was prepared, and the CD spectrum was collected from 480–230 nm at a rate of 50 $\mu\text{M min}^{-1}$ at 25 $^\circ\text{C}$. The re-

ported spectra are an average of at least five scans. To obtain the stoichiometry of each complex, a DNA solution was titrated with a compound solution, and the induced CD (ICD) of the bound compound was followed at the maximum wavelength.

Biosensor surface plasmon resonance (SPR): SPR measurements were performed in a four-channel Biacore 2000 optical biosensor system (GE Healthcare). The 5'-biotin-labeled DNA sequences (A_5 and ATATA hairpins, in Scheme 1) were immobilized onto streptavidin-coated sensor chips (Biacore), as previously described.^[34,35] Three flow cells were used to immobilize the DNA oligomer samples, while a fourth cell was left blank as a control. The SPR experiments were performed at 25 $^\circ\text{C}$ in filtered, degassed CAC buffer. Steady-state binding analysis was performed with multiple injections of different compound concentrations over the immobilized DNA surface at a flow rate of 25 $\mu\text{L min}^{-1}$ and 25 $^\circ\text{C}$. Solutions of known AIA concentration were injected through the flow cells until a constant steady-state response was obtained. Solution flow was then replaced by buffer flow resulting in dissociation of the complex. The reference response from the blank cell was subtracted from the response in each cell containing DNA to give a signal (RU) that is directly proportional to the amount of bound compound. The predicted maximum response per bound compound in the steady-state region (RU_{max}) was determined from the DNA molecular weight, the amount of DNA in the flow cell, the compound molecular weight, and the refractive index gradient ratio of the compound and DNA, as previously described.^[36,37] The number of binding sites and the equilibrium constant were obtained from fitting plots of RU versus C_{free} . Binding results from the SPR experiments were fit with either a single-site ($K_2=0$) or with a two-site model [Eq. (2)]:

$$r = \frac{K_1 C_{\text{free}} + 2K_1 K_2 C_{\text{free}}^2}{1 + K_1 C_{\text{free}} + K_1 K_2 C_{\text{free}}^2} \quad (2)$$

here r represents the moles of bound compound per mole of DNA hairpin duplex, K_1 and K_2 are macroscopic binding constants, and C_{free} is the concentration of free compound in equilibrium with the complex.

Purification and radiolabeling of DNA restriction fragments and DNase I footprinting: DNase I footprinting experiments were performed essentially as described previously.^[34,35] Complementary 5'-end-phosphorylated oligonucleotides containing A_5 and ATATA sites (underlined) 5'-CGGTAC CAGATC TTCTAG GAAAAA CGGCTC GATATA GCAGGC TGGATC CCG and 5'-GATCCG GGATCC AGCCTG CTATAT CGAGGC GTTTTT CCTAGA AGATCT GGTACC GACT were synthesized by Eurogentec (Seraing, Belgium) and hybridized by heating the mixture at 95 $^\circ\text{C}$ for 5 min followed by a slow temperature decrease to room temperature. The double-stranded DNA was then subcloned in pUC19 previously opened at *SacI* and *BamHI* sites. The 81 bp DNA fragment encompassing this subcloned sequence was obtained from *EcoRI* and *PstI* double digestion of this new pUC19–ATATA vector and 3'-end labeled by using α -[^{32}P]dATP (3000 Ci mmol $^{-1}$ each, PerkinElmer) and ten units of Klenow enzyme (BioLabs, Évry, France) for 30 min at 37 $^\circ\text{C}$, separated and isolated from the plasmid remnant by using a 6% native polyacrylamide gel, as previously described.^[38] Increasing concentrations (as indicated in the figure legends) of the various tested compounds were incubated for 15 min at 37 $^\circ\text{C}$ with the radiolabeled DNA fragments prior to digestion with DNase I (0.001 unit mL $^{-1}$, Sigma) for 3 min in digestion buffer (20 mM NaCl, 2 mM MgCl_2 , 2 mM MnCl_2 , pH 7.3). Reaction was stopped by freeze-drying and lyophilization. The cleaved DNA fragments were dissolved in formamide-contain-

ing denaturing loading buffer (4 μ L), heat-denatured for 4 min at 90 °C, and rapidly chilled on ice prior to electrophoresis on a 8% denaturing polyacrylamide gel. The gels were then soaked in 10% acetic acid, transferred to Whatman 3 MM paper, and dried under vacuum at 80 °C. Dried gels were exposed overnight on storage screens and scanned by using a Molecular Dynamics STORM 860. Quantification of the cleaved bands was performed by using Image Quant 4.1 software.

X-ray crystallography: The oligonucleotide sequence, d(CGCGAA TTCGCG)₂, was purchased from DNA Technology A/S (Risskov, Denmark), and DB1880 was used as the hydrochloride salt without any further purification. The final dsDNA stock solution was 3.0 mM by annealing (6.0 mM in single-stranded DNA in 20 mM sodium cacodylate, pH 6.5) through heating the mixture to 85 °C for 15 min and then cooling it to room temperature overnight. DNA complex crystals were grown by the hanging-drop, vapor-diffusion method. A successful crystallization experiment typically comprised annealed dsDNA (1 μ L, 1.5 mM) with ligand DB1880 (2.25 mM), mixed with reagent solution (1 mL; 7% 2-methylpentane-2,4-diol (MPD), 140 mM MgCl₂, 20 mM sodium cacodylate, pH 6.5). The hanging drop was equilibrated against a well containing 50% MPD. Crystals grew in one week at 10 °C. A dataset was collected at 105 K from a single flash-frozen crystal by using an Oxford Diffraction Xcalibur NovaT X-ray diffractometer. The data were processed and scaled by using CrysAlisPro (Oxford Diffraction) and Scala (CCP4 suite).

The structure was solved by molecular replacement using the REFMAC 5.5.0109 program (CCP4), using the DB1880-d(CGCGAA TTCGCG)₂ complex structure (PDB ID: 2B3E)^[46] as a model, and refined by using REFMAC 5.5.0109. Data collection and refinement statistics are shown in Table 3. The DB1880 ligand and Mg²⁺ ion could be clearly seen in the initial σ_A -weighted $2F_o - F_c$ electron-density maps. The final model (including solvent molecules) was refined by using data between 22.66 and 1.90 Å, with final *R* and *R*_{free} values of 0.163 and 0.240, respectively.

Structural comparisons of free compounds: Molecular modeling studies were initiated by conformation analysis of the tested com-

pounds in Table 1 with a molecular mechanics MMFF approximation level with the Spartan'10 software package (Wavefunction Inc.). The Spartan'10 software package was employed to optimize the final geometry by using ab initio calculations with B3LYP DFT at the 631G* approximation level. The molecular energy was calculated by employing the Hartree–Fock approximation also at the 631G* level. To evaluate electrostatic and structural properties, MEP color-coded maps were generated in the range from 250 (deep red) to 700 kJ mol⁻¹ (deep blue) and superimposed onto the molecular surface; red represents regions with the most negative electrostatic potential, blue represents the most positive, and green represents regions of zero potential. Negative electrostatic potential corresponds to attraction of a proton by the aggregate electron density in the molecule; positive electrostatic potential corresponds to repulsion of a proton by the atomic nuclei.

Molecular docking: Molecular docking studies were performed with the SYBYL-X1.2 software package on a Windows 8 processor Workstation.^[47] The Surflex-Dock module of the SYBYL software uses a surface-shape-based method that aligns each test ligand to a "protomol".^[48–51] The protomol consists of a series of molecular fragments that characterize the surface properties of the target active site, including steric effects, hydrogen bond acceptors and hydrogen bond donors.^[48] Docking of the selected compounds (Table 1) into the DNA minor groove consisted of three steps: 1) preparation of the 3D structure of a DNA sequence and construction of the protomol, 2) preparation of each compound, and 3) docking of each compound into the protomol.

The X-ray crystal structure of the DB1880–DNA complex (PDB ID: 3OIE) was used to generate the protomol. The bound compound was extracted from the DNA crystal structure and was used as the ligand for protomol generation in the following Surflex-docking steps. After the crystallographic water molecules and metal ions had been removed and hydrogen atoms had been added, the modified DNA sequences were minimized for a maximum of 100 iterations with a termination gradient of 0.01 kcal mol⁻¹ Å⁻¹. The Surflex-dock module of the SYBYL software suite was then implemented, and the protomol was generated by using a ligand-based approach with the extracted AIA reference compound from the crystal structure. The two important factors that can affect the size and extent of the protomol generated are "proto_thresh" and "proto_bloat". "Proto_thresh" determines how far the protomol extends into the target site; "proto_bloat" affects how far the protomol extends outside the concavity.^[47,50] For the purpose of these experiments, "proto_thresh" was set to 0.2 and "proto_bloat" was left at the default values of 0.

SYBYL-X1.2 software was then employed to construct the test compounds in three-dimensional space. They underwent a short MD simulation of 1 ns at a constant temperature and volume (NTV).^[52] Briefly, 1) the system temperature was set to 300 K with a coupling constant of 100 fs, 2) a Maxwell–Boltzmann distribution was employed for initial atom velocities, 3) the nonbonded pair list was updated every 25 fs, and 4) the duration of the MD simulations in vacuo was 1 ns with a time step of 100 fs and a snapshot every 1000 fs. Snapshots from the MD simulation displayed several low-energy structures. These were minimized to convergence by using the Tripos force field with conjugate gradient algorithm, and Gasteiger–Hückel charges.^[46] The termination gradient was 0.01 kcal mol⁻¹ Å⁻¹, and the maximum iterations were 10⁴. The Surflex-dock GeomX module of the SYBYL software suite was then implemented to dock each compound into the protomol. Each docking starts from six multiple initial poses to ensure good search coverage.

Table 3. Data collection and refinement statistics for the DB1880–d(CGCGAA TTCGCG)₂ complex crystal structure.

Data collection	
sequence	d(CGCGAA TTCGCG) ₂
space group	<i>P</i> 2 ₁ 2 ₁ 2 ₁
unit cell dimensions	
<i>a</i> , <i>b</i> , <i>c</i> [Å]	24.11, 38.42, 66.21
resolution [Å]	66.19–1.71
<i>R</i> _{int} [%] overall	3.04
<i>I</i> / σ	37.88
completeness [%]	74.10
redundancy	1.9
Refinement	
resolution limits [Å]	22.7–1.90
no. of reflections	4962
completeness [%]	95.1
<i>R</i> _{work} / <i>R</i> _{free} [%]	16.3/24.0
no. of atoms	672
no. of ions	1
no. of waters	136
overall B-factor [Å ²]	21.8
RMS deviations	
bond lengths [Å]	0.01
bond angles [°]	1.2
PDB ID	3OIE

Acknowledgements

This work was supported by NIH grant AI064200 and by The Bill and Melinda Gates Foundation through a subcontract with the Consortium of Parasitic Drug Development (W.D.W. and D.W.B.), Cancer Research UK grant C129/A4489 (to S.N.), the Fonds Européen de Développement Régional (FEDER, European Community) and the Région Nord-Pas de Calais, the Ligue Nationale Contre le Cancer (Comité du Nord, Septentrion), the Association Laurette Fugain and the Institut pour la Recherche sur le Cancer de Lille (IRCL) (to M.H.D.C.). R.N. thanks the IRCL for a post-doctoral fellowship.

Keywords: arylimidamides • DNA • minor-groove binders • molecular modeling • X-ray crystallography

- [1] J. R. Coura, P. A. Viñas, *Nature* **2010**, *465*, S6–S7.
- [2] W. Apt, *Drug Des. Dev. Ther.* **2010**, *243*–253.
- [3] W. de Souza, *Microbes Infect.* **2007**, *9*, 544–545.
- [4] C. J. Schofield, J. Jannin, R. Salvatella, *Trends Parasitol.* **2006**, *22*, 583–588.
- [5] M. N. Soeiro, K. Werbovetz, D. W. Boykin, W. D. Wilson, M. Z. Wang, A. Hemphill, *Parasitology* **2013**, *140*, 929–951.
- [6] M. P. Barrett, D. W. Boykin, R. Brun, R. R. Tidwell, *Br. J. Pharmacol.* **2007**, *152*, 1155–1171.
- [7] W. D. Wilson, B. Nguyen, F. A. Tanius, A. Mathis, J. E. Hall, C. E. Stephens, D. W. Boykin, *Curr. Med. Chem. Anticancer Agents* **2005**, *5*, 389–408.
- [8] W. D. Wilson, F. A. Tanius, A. Mathis, D. Tevis, J. E. Hall, D. W. Boykin, *Biochimie* **2008**, *90*, 999–1014.
- [9] M. C. Machado Motta, *Curr. Pharm. Des.* **2008**, *14*, 847–854.
- [10] A. M. Mathis, A. S. Bridges, M. A. Ismail, A. Kumar, I. Francesconi, M. Anbazhagan, Q. Y. Hu, F. A. Tanius, T. Wenzler, J. Saulter, W. D. Wilson, R. Brun, D. W. Boykin, R. R. Tidwell, J. E. Hall, *Antimicrob. Agents Chemother.* **2007**, *51*, 2801–2810.
- [11] D. S. Tevis, A. Kumar, C. E. Stephens, D. W. Boykin, W. D. Wilson, *Nucleic Acids Res.* **2009**, *37*, 5550–5558.
- [12] T. A. Shapiro, P. T. Englund, *Proc. Natl. Acad. Sci. USA* **1990**, *87*, 950–954.
- [13] O. Vázquez, M. I. Sánchez, J. Martínez-Costas, M. E. Vázquez, J. L. Mascareñas, *Org. Lett.* **2010**, *12*, 216–219.
- [14] M. I. Sánchez, O. Vázquez, J. Martínez-Costas, M. E. Vázquez, J. L. Mascareñas, *Chem. Sci.* **2012**, *3*, 2383–2387.
- [15] T. Wenzler, D. W. Boykin, M. A. Ismail, J. E. Hall, R. R. Tidwell, R. Brun, *Antimicrob. Agents Chemother.* **2009**, *53*, 4185–4192.
- [16] J. K. Thuita, M. Z. Wang, J. M. Kagira, C. L. Denton, M. F. Paine, R. E. Mdachi, G. A. Murilla, S. Ching, D. W. Boykin, R. R. Tidwell, J. E. Hall, B. Brun, *PLoS Neglected Trop. Dis.* **2012**, *6*, e1734.
- [17] D. W. Boykin, A. Kumar, J. E. Hall, B. C. Bender, R. R. Tidwell, *Bioorg. Med. Chem. Lett.* **1996**, *6*, 3017–3020.
- [18] J. H. Ansele, M. Anbazhagan, R. Brun, J. D. Easterbrook, J. E. Hall, D. W. Boykin, *J. Med. Chem.* **2004**, *47*, 4335–4338.
- [19] R. R. Tidwell, D. W. Boykin in *DNA and RNA Binders: From Small Molecules to Drugs*, Vol. 2 (Eds.: M. Demeunynck, C. Bailly, W. D. Wilson), Wiley-VCH, Weinheim, **2003**, pp. 414–460.
- [20] M. F. Paine, M. Z. Wang, C. N. Generaux, D. W. Boykin, W. D. Wilson, H. P. De Koning, C. A. Olson, G. Pohlig, C. Burri, R. Brun, G. A. Murilla, J. K. Thuita, M. P. Barrett, R. R. Tidwell, *Curr. Opin. Invest. Drugs* **2010**, *11*, 876–883.
- [21] A. Mayence, J. J. Eynde, F. M. Krogstad, D. J. Krogstad, M. T. Cushion, T. L. Huang, *J. Med. Chem.* **2004**, *47*, 2700–2705.
- [22] H. Denise, M. P. Barrett, *Biochem. Pharmacol.* **2001**, *61*, 1–5.
- [23] R. A. Hunt, M. Munde, A. Kumar, M. A. Ismail, A. A. Farahat, R. K. Arafa, M. Say, A. Batista-Parra, D. S. Tevis, D. W. Boykin, W. D. Wilson, *Nucleic Acids Res.* **2011**, *39*, 4265–4274.
- [24] M. Rettig, M. W. Germann, S. Wang, W. D. Wilson, *ChemBioChem* **2013**, *14*, 323–331.
- [25] N. S. Carter, B. J. Berger, A. H. Fairlamb, *J. Biol. Chem.* **1995**, *270*, 28153–28157.
- [26] M. N. C. Soeiro, K. Werbovetz, D. W. Boykin, W. D. Wilson, M. Z. Wang, A. Hemphill, *Parasitology* **2013**, *140*, 929–951.
- [27] C. E. Stephens, R. Brun, M. M. Salem, K. A. Werbovetz, F. Tanius, W. D. Wilson, D. W. Boykin, *Bioorg. Med. Chem. Lett.* **2003**, *13*, 2065–2069.
- [28] C. F. Silva, M. M. Batista, R. A. Mota, E. M. de Souza, C. E. Stephens, P. Som, D. W. Boykin, N. Soeiro, *Biochem. Pharmacol.* **2007**, *73*, 1939–1946.
- [29] M. Z. Wang, X. H. Zhu, A. Srivastava, Q. Liu, J. M. Sweat, T. Pandharkar, C. E. Stephens, E. Riccio, T. Parman, M. Munde, S. Mandal, R. Madhubala, R. R. Tidwell, W. D. Wilson, D. W. Boykin, J. E. Hall, D. E. Kile, K. A. Werbovetz, *Antimicrob. Agents Chemother.* **2010**, *54*, 2507–2516.
- [30] C. F. Silva, M. B. Meuser, E. M. De Souza, M. N. Meirelles, C. E. L. Stephens, P. Som, D. W. Boykin, N. Soeiro, *Antimicrob. Agents Chemother.* **2007**, *51*, 3803–3809.
- [31] X. H. Zhu, Q. Liu, S. H. Yang, T. F. Parman, C. E. Green, J. C. Mirsalis, M. de Nazaré Correia Soeiro, E. Mello de Souza, C. F. da Silva, D. da Gama Jaen Batista, C. E. Stephens, M. Banerjee, A. A. Farahat, M. Munde, W. D. Wilson, D. W. Boykin, M. Z. Wang, K. A. Werbovetz, *Antimicrob. Agents Chemother.* **2012**, *56*, 3690–3699.
- [32] W. D. Wilson, F. A. Tanius, M. Fernandez-Saiz, C. T. Rigl in *Methods in Molecular Biology, Vol. 90: Evaluation of Drug–Nucleic Acid Interactions by Thermal Melting Curves* (Ed.: K. R. Fox), Humana, Totowa, **1998**, pp. 219–240.
- [33] W. D. Wilson, S. Mizan, F. A. Tanius, S. Yao, G. Zon, *J. Mol. Recognit.* **1994**, *7*, 89–98.
- [34] B. Nguyen, F. A. Tanius, W. D. Wilson, *Methods* **2007**, *42*, 150–161.
- [35] Y. Liu, W. D. Wilson in *Methods in Molecular Biology, Vol. 613: Quantitative Analysis of Small Molecule–Nucleic Acid Interactions with a Biosensor Surface and Surface Plasmon Resonance Detection* (Ed.: K. R. Fox), Humana, Totowa, **2010**, pp. 1–23.
- [36] R. Nanjunda, M. Munde, Y. Liu, W. D. Wilson in *Methods for Studying DNA/Drug Interactions*, (Eds.: M. Wanunu, Y. Tor), CRC Press, Boca Raton, **2011**, Chapter 4.
- [37] T. M. Davis, W. D. Wilson, *Methods Enzymol.* **2001**, *340*, 22–51.
- [38] P. Peixoto, Y. Liu, S. Depauw, M. P. Hildebrand, D. W. Boykin, C. Bailly, W. D. Wilson, M. H. David-Cordonnier, *Nucleic Acids Res.* **2008**, *36*, 3341–3353.
- [39] Y. Liu, A. Kumar, S. Depauw, R. Nhili, M.-H. David-Cordonnier, M. P. Lee, M. A. Ismail, A. A. Farahat, M. Say, S. Chackal-Catoen, A. Batista-Parra, S. Neidle, D. W. Boykin, W. D. Wilson, *J. Am. Chem. Soc.* **2011**, *133*, 10171–10183.
- [40] D. G. Brown, M. R. Sanderson, J. V. Skelly, T. C. Jenkins, T. Brown, E. Garman, D. Stuart, S. Neidle, *EMBO J.* **1990**, *9*, 1329–1334.
- [41] C. A. Laughton, F. Tanius, C. M. Nunn, D. W. Boykin, W. D. Wilson, S. Neidle, *Biochemistry* **1996**, *35*, 5655–5661.
- [42] B. Nguyen, S. Neidle, W. D. Wilson, *Acc. Chem. Res.* **2009**, *42*, 11–21.
- [43] S. Neidle, *Nat. Prod. Rep.* **2001**, *18*, 291–309.
- [44] D. Wei, W. D. Wilson, S. Neidle, *J. Am. Chem. Soc.* **2013**, *135*, 1369–1377.
- [45] C. E. Stephens, F. Tanius, S. Kim, W. D. Wilson, W. A. Schell, J. R. Perfect, S. G. Franzblau, D. W. Boykin, *J. Med. Chem.* **2001**, *44*, 1741–1748.
- [46] N. H. Campbell, D. A. Evans, M. A. Lee, G. N. Parkinson, S. Neidle, *Bioorg. Med. Chem. Lett.* **2006**, *16*, 15–19.
- [47] SYBYL Molecular Modeling Software, Version X1.2, Tripos Inc., St. Louis, MO, **2010**.
- [48] A. N. Jain, *J. Med. Chem.* **2003**, *46*, 499–511.
- [49] A. N. Jain, *J. Comput.-Aided Mol. Des.* **2007**, *21*, 281–306.
- [50] P. A. Holt, J. B. Chaires, J. O. Trent, *J. Chem. Inf. Model.* **2008**, *48*, 1602–1615.
- [51] M. M. Dailey, C. Hait, P. A. Holt, J. M. Maguire, J. B. Meier, M. C. Miller, L. Petraccone, J. O. Trent, *Exp. Mol. Pathol.* **2009**, *86*, 141–150.
- [52] C. J. Collar, X. Zhu, K. Werbovetz, D. W. Boykin, W. D. Wilson, *Bioorg. Med. Chem.* **2011**, *19*, 4552–4561.

Received: September 25, 2013

Published online on December 9, 2013